Journal of Materials Chemistry A

Accepted Manuscript

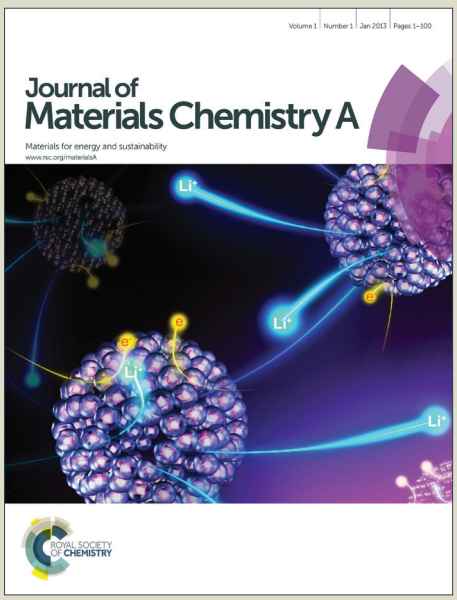

ROYAL SOCIETY OF CHEMISTRY

www.rsc.org/materialsA

Journal Name

ARTICLE

Nanostructured 2D MoS_2 Honeycomb and Hierarchical 3D Marigold Nanoflower of $CdMoS_4$ for Hydrogen Production under Solar Light

Received 00th January 20xx,
Accepted 00th January 20xx

DOI: 10.1039/x0xx00000x

www.rsc.org/

Sunil R. Kadam,[a] Dattatray J. Late,[b] Rajendra P. Panmand,[a] Milind V. Kulkarni,[a] Latesh K. Nikam,[a] Suresh W. Gosavi,[c] Chan J. Park*,[d] Bharat B. Kale*[a]

The unique two dimensional (2D) honeycomb layered MoS_2 nanostructure and hierarchical 3D marigold nanoflowers of $CdMoS_4$ were architectured using a template free facile solvothermal method. The MoS_2 depicts the sheet like morphology with lateral dimension 5-10 µm and thickness ~ 200 nm with honeycomb nanostructure architecture via self-assembling of vertically grown thin hexagonal nanosheets with thickness 2-3 nm. The 3D architectured $CdMoS_4$ marigold nanoflowers comprised with thin nano petals with lateral dimension 1-2 µm and thickness of few nm. The $CdMoS_4$ and MoS_2 were confer hydrogen (H_2) production rate, 25445 and 12555 µMoleh^{-1}g^{-1}, respectively. The apparent quantum yield of hydrogen production was observed to be 35.34 and 17.18 % for $CdMoS_4$ and MoS_2, respectively. The 3D nanostructure marigold flowers of $CdMoS_4$ and honeycomb like 2D nanostructure of MoS_2 responsible for higher photocatalytic activity due to inhibition in the charge carrier recombination. The prima fascia observation of H_2 production shows that the ternary semiconductor confers enhanced photocatalytic activity for H_2 generation due to unique structure. Such structures can be architecture and implemented for other transition metal dichalcogenide based ternary materials for enhanced photocatalytic and other applications.

1 Introduction

Transition metal dichalcogenides (TMDCs) such as 2D honeycomb like layered MoS_2 and other semiconductor nanostructure materials have immense importance due to their size and shape dependent enhanced properties for various energy and nanoelectronics device applications.[1-3] Significantly, 1 to 3D nanostructure materials have been widely utilized for the advance energy applications like solar cells, batteries, photocatalysis and for optoelectronic applications.[3-6] Particularly, in photocatalysis the nanostructure semiconductors and especially hierarchical nanostructures are playing crucial role in the drastic enhancement in the efficiency due to the control on recombination of photo generated charge carriers.[7]

The H_2 is one of the best options for the future as a clean and direct fuel source to solve our energy related problems and need. Moreover, H_2 can be produced from several different sources such as water, biomass, natural gas or coal.[8-10] Currently, the most commonly used and practically efficient methods for H_2 production are coal gasification and steam reforming of methane. But both the methods are energy rigorous with undesirable for environmental related issues and problems.[8,11] The environment pollutant and corrosive H_2S is continuously released (10-15% as waste) by oil refineries is a global intimidation to the environment. The present Claus process is a commercial process for H_2S utilization to produce liquid sulphur rather than H_2 which is laborious and highly expensive.[12] Hence, the generation of clean H_2 energy from the decomposition of abundant environmental pollutant H_2S has been more significance. The great challenge is to design a catalyst system that can electively use sunlight and H_2S to generate H_2. Heterogeneous photocatalysts plays an important role for the conversion of photon energy into chemical energy and for decomposing the organic contaminants as well as H_2 generation.[13,14] There are reports on the development of ultra-violet active photocatalyst for H_2 production based on oxide nanomaterials.[15-16] But the problem with oxide based catalyst such as TiO_2, ZnO, ZnO/ZnS, have wide band gap and show activity under UV light only (>3.0 eV) which is only 5% of the solar spectrum and did not show good photocatalytic activity in the visible light.[17,18] Furthermore, there are attempts on development of doped oxide nanomaterials for visible light active photocatalyst such as Fe_2O_3, Bi_2O_3, $BiVO_4$, MoO_3, $ZnCo_2O_4$, N doped TiO_2/ZnO *etc.* for H_2 generation.[18-24] However, the problem with these materials is their poor stability. Hence, researchers are concentrating for the development of stable and visible light active efficient photocatalyst for H_2 production from water as well as H_2S. The visible light active semiconductor sulphide photocatalyst have been reported which includes, CdS, CuS, In_2S_3, Bi_2S_3 etc.[13,25-29] Among all the sulfides photocatalyst, CdS was found to be good visible light active photocatalyst, but due to photocorrosion and stability of CdS limits its commercial use as a visible light active photocatalyst. Hence, further researchers have tried to develop hetero structures of CdS-ZnO, CdS-TiO_2 *etc.* as a visible light active photocatalyst for H_2 generation.[30-31]

Recently, we have also investigated cadmium based ternary chalcogenide as a visible light active photocatalysts.[32] These ternary systems observed to be efficient as compare to CdS and other sulfide. Further, we have also attempted H_2 generation via H_2S decomposition using nanostructure cadmium indium sulfide and zinc indium sulfide ternary semiconductor photocatalyst.[32-34] The hierarchical nanostructures of such ternary systems are expected to be efficient photocatalyst due to the high surface area and large aspect ratio. Hence, we focused the innovative approach for the synthesis of such hierarchical nanostructures as a visible light active photocatalyst for H_2 production.

In this context, we have attempted to develop template free synthesis of ternary $CdMoS_4$ as well as pristine MoS_2 nanosheet with 2D honeycomb nanostructure by simple solvothermal method. Considering their optical properties, they have ability to be used as a visible light active photocatalyst for H_2 production from photocatalytic H_2S splitting. In the present investigation, we have demonstrated the synthesis of 3D hierarchical nanostructure marigold $CdMoS_4$ nanoflower and 2D MoS_2 honeycomb nano sheet as a photocatalyst for H_2 production from H_2S under solar light which is hitherto un-attempted.

2. EXPERIMENTAL METHODS

2.1 Material Preparation

All chemicals were purchased from Fisher Scientific with (Purity 99 %). All the chemicals were analytic grade and were used without any further purification. Cadmium nitrate (2 mmol) dissolved in methanol (40-50 ml) and ammonium molybdate (20 ml) dissolved in methanol by addition of nitric acid drop by drop with constant stirring for 10 minutes as long as to see the clear solution. Next we followed the drop wise addition of dissolved cadmium nitrate solution into the ammonium molybdate solution with constant stirring for another 10 min. After complete addition, it was allow to stir for 15 more minutes with drop wise addition of dissolved thiourea, followed by stirring for 15 more minutes. The pH of the solution is measured to be 1. The solution was then transferred in teflon coated hydrothermal reactor and kept for 48 hours at 150 ^oC. After completion of reaction, reactor was allowed to cool down to room temperature naturally, followed by washing of the product with distilled water and filtered using 0.41 whatman filter paper. Further, products were washed using AR grade ethanol for several times and then dried at 80 ^oC for 4 hours in oven.

2.2 Photocatalytic Activity

2.2.1 H_2S Splitting

For photocatalytic studies, the cylindrical quartz reactor filled with 750 ml 0.25 M aqueous KOH. At room temperature, the vigorously stirred suspension was purged with argon for 1 h and then hydrogen sulphide (H_2S) generated in kipps apparatus was bubbled through the solution for about 1 h. Each experiment was carried out in 750 ml of KOH solution (0.25 M) with H_2S flow 2.5 ml min^{-1}. The annealed MoS_2 and $CdMoS_4$ photocatalyst were introduced as a suspension into a reactor and irradiated with Xe-lamp light source (LOT ORIEL GRUPPE, EUROPA, LSH302, for Xe lamp spectrum) of intensity 300 W. The generated H_2 was collected in the graduated eudiometric tube. The purity of the collected gas was analyzed by gas chromatograph (Model Schimadzu GC-14B, MS-5 Å column, TCD, Ar carrier). Apparent quantum yield (QY) was determined with measuring intensity of light with Lux meter (Lutron LX-107HA) and it was placed in front of 300 W Xe light source to obtain the correct wavelength. Apparent quantum yield (AQE) was calculated according to the following equation:

$$\text{AQE } (\%) = \frac{\text{Number of } H_2 \text{molecules evolved x 2}}{\text{Number of incident photon}} \text{x } 100$$

2.2.2 Water Splitting

The photocatalytic water splitting was carried out by using 100 ml double distilled water in 250 ml round bottom flask and 25 ml methanol as a sacrificial reagent. The annealed MoS_2 and $CdMoS_4$ catalyst was added with 1 wt% preloaded platinum as a co-catalyst. Argon gas was purged through this reaction mixture in order to remove the dissolved gases. The 250 ml round bottom flask was connected to the graduated measuring gas collector tube. The gas collector tube has septum arrangement to get rid of the evolved gas through the gas tight syringe for measure the amount of gas evolved. The all assembly was arranged in a wooden box and round bottom flask containing reaction mixture was irradiated with by 400 W mercury vapour lamp. The mercury vapour lamp was fitted with quartz condenser having arrangement for water circulation in order to absorb the IR radiation which minimizes the overheating effect. As soon as the lamp was switched on, the photocatalytic splitting of water was started and generated H_2 was collected in a graduated measuring gas collector. The amount of gas evolved was noted with time. The purity of the collected gas was analyzed by gas chromatograph (Model Schimadzu GC-14B, MS-5 Å column, TCD, Ar carrier).

2.3 Material Characterisation

The crystalline phases were investigated using X-ray powder diffraction (XRD) technique (XRD-D8, Advance, Bruker-AXS). Further, Cd, Mo and S content and oxidation state of element were examined using X-ray photoelectron spectroscopy (XPS, ESCA-3000, VG Scientific Ltd., England). Room temperature Raman spectroscopy were performed using a HR 800-Raman Spectroscopy, Horiba JobinYvon, France, with an excitation laser wavelength of 632.81 nm by a coherent He–Ne ion laser and a liquid nitrogen cooled detector to collect and process the scattered data. The optical properties of the powder samples were studied using an UV-visible-near infrared spectrometer (UV-VIS-NIR, Perkin Elmer Lambda-950). Photoluminescence properties of samples were analysed by using HORIBA Flurolog 3 spectroflurometer. The morphologies of the as synthesized and annealed sample were

investigated by field emission scanning electron microscopy (FESEM, Hitachi, S-4800). For TEM (JEOL, 2010F instrument). The visible light source used for the photocatalytic activity was Xe-lamp light source (LOT ORIEL GRUPPE, EUROPA, LSH302, for Xe lamp spectrum) of intensity 300 W. The purity of the collected gas was analyzed by gas chromatograph (Model Schimadzu GC-14B, MS-5 Å column, TCD, Ar carrier).

3. RESULTS AND DISCUSSION

The MoS_2 and $CdMoS_4$ nanostructures have been synthesized by facile solvothermal method. For the structural and phase comparison, the CdS has also been synthesized at an identical condition. The structural phase formation of as prepared CdS, MoS_2, $CdMoS_4$ and annealed $CdMoS_4$ and MoS_2 are investigated by X-ray Diffraction (XRD) and it is depicted in Figure 1a-d. The XRD of as prepared CdS, $CdMoS_4$ and MoS_2 are shown in Figure 1a. The XRD of as prepared CdS sample shows the formation of typical cubic structure, which matches very well with the reported JCPDS data card No. 01-075-1546. The XRD of as prepared MoS_2 shows the peaks at 2θ=13.0°, 16.5°, 25.6°, 33.5°, 44.7°, 60.5° and 70.5°. After annealing the same sample at 400°C, depict slight shift in peak position from 2θ=13.0° to 13.8 (3hrs) and 14.0° (4 hrs) which indicates slight structural deformation in MoS_2 as shown in Figure 1c and which matches well with the reported hexagonal MoS_2 having JCPDS data card No. 00-009-0312. The as prepared $CdMoS_4$ is annealed at 400 °C for 3 and 4 hours, respectively and their corresponding XRD were shown in Figure 1b. It is observed that the XRD peak at 2θ=13° in as prepared $CdMoS_4$ sample is slightly shifted to 13.5° and 14.0° after annealing at 400 °C for 3 and 4 hours, respectively which indicates slight deformation in the crystal structure. It is observed that after annealing the samples, phase formation of MoS_2 and $CdMoS_4$ takes place which is confirmed by XRD and were depicted in Figure 1d along with as prepared CdS sample. The XRD of annealed $CdMoS_4$ sample has been analyzed using powder 4–DICVOLE-91 software, which shows the formation of monoclinic structure (a=9.04588 A°, b=4.01129 A°, c=6.29441 A° and β=92.739°, V=228.136. (A°) 3) and matches well with the reported literature.[35,36]

The morphological investigations of the as synthesized CdS were performed by FESEM and were shown in ESI S-1 (Figure S-1a-d). From FESEM images, it is clearly observed that the formation of the cauliflower (1 µm) like morphology via assembling of tiny nanoparticles of size 10-15 nm. Figure 2a-d shows FESEM images of as prepared and annealed MoS_2, where one can clearly see the formation of long ~5 µm mesoporous nanosheets with honeycomb like morphology. It is noteworthy that such unique honeycomb nanostructure of MoS_2 using solvothermal process is hitherto unattempted. Interestingly, the stacking of honeycomb sheets was also observed. Overall, we found the stacking of 2-3 sheets, occasionally. The thickness of sheet is observed to be ~200 nm (See inset of Figure 2b). The thickness of the individual comb cell wall is observed to be ~10 nm in size (Figure 2b,d). More significantly, the cavities of honeycomb MoS_2 generated via vertical growth of nanosheets were also hexagonal in shape and the overall diameter of the cavities is around 40-50nm. The depths of the cavities were also measured to be 200 nm as per the layer thickness. Overall, FESEM observations depicts that there is not much change in the morphology of the as prepared and annealed MoS_2 sample.

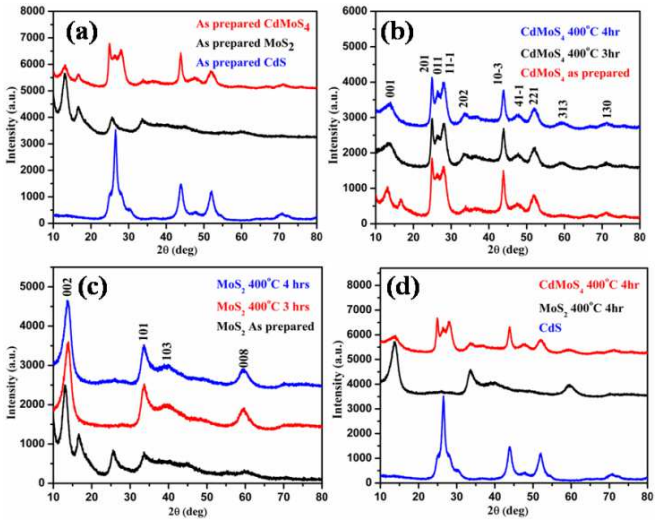

Figure 1. (a) XRD of as prepared CdS, $CdMoS_4$ and MoS_2. **(b)** XRD of $CdMoS_4$ as a function of annealing at 400 °C for 3 hrs and 4 hrs. **(c)** XRD of MoS_2 as a function of annealing at 400 °C for 3 hrs and 4 hrs. **(d)** XRD spectra of CdS and annealed $CdMoS_4$ and MoS_2.

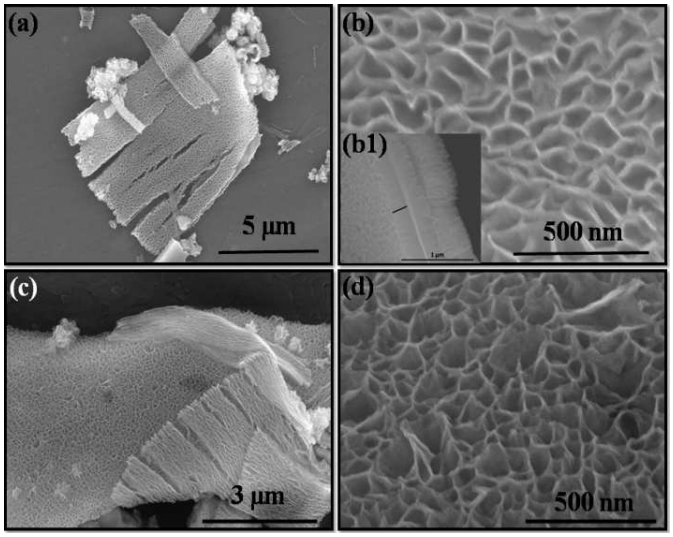

Figure 2. FESEM images of **(a-b)** as synthesized MoS_2 and **(c-d)** annealed MoS_2 at 400 °C.

Further, the TEM investigations were performed in order to examine the morphology and crystalline nature of the annealed MoS_2 sample (Figure 3a-d). The hexagonal honeycombs like structure were also noticed in the TEM. The corresponding TEM images of annealed MoS_2 sample shows ordered mesoporous honeycomb structure with hexagonal cavities of 40-50 nm (Figure 3a), which is also in good agreement with our FESEM analysis. Figure 3a shows the High resolution (HR) TEM images taken from the edge of the nanosheets, which

provides more detailed structural information. The lattice spacing observed to be 0.266 nm which corresponds to the (002) plane of hexagonal MoS_2 (Figure 3c), and is in consistent with XRD results. Figure 3d shows the selected area electron diffraction (SAED) pattern of annealed MoS_2 sample which clearly shows a highly crystalline nature of sample attributed to the MoS_2 2H phase.

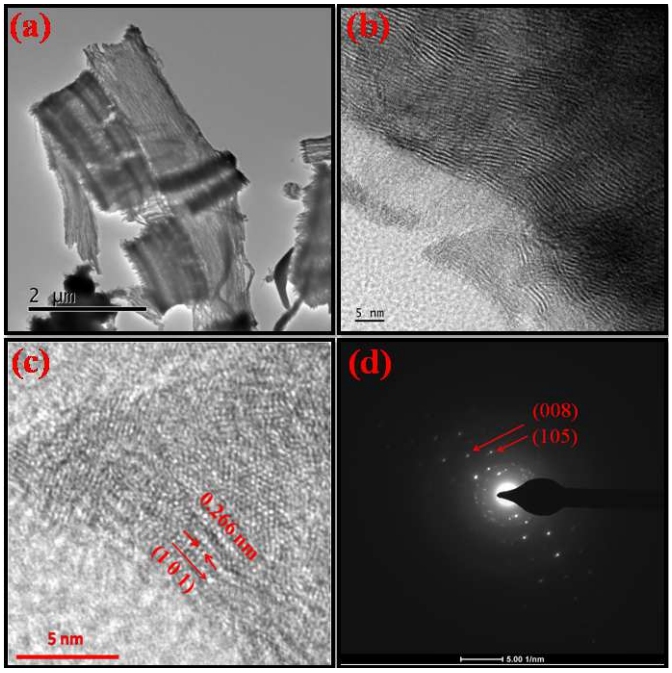

Figure 3. (a) Low resolution and **(b, c)** high resolution TEM images of annealed MoS_2 nanosheet sample at 400 °C and **(d)** corresponding SAED pattern.

The morphological investigations of as prepared and annealed $CdMoS_4$ sample were also carried out by FESEM. Figure 4 (a-b & c-d) shows the FESEM images of the as prepared and annealed $CdMoS_4$ sample, respectively**.** Further, FESEM results reveals the formation of porous marigold nanoflower like morphology. The magnified FESEM images (Figure 4b, d) indicate the detailed marigold nanoflower like structure instead of honeycomb which was observed in case of MoS_2. Interestingly, marigold nanoflower like morphology composed of large number of thin nanopetals as building blocks. The as prepared $CdMoS_4$ sample (Figure 4a-b) shows compact flower like structure and annealed $CdMoS_4$ sample (Figure 4c-d) shows puffy nanoflowers. This is quite obvious that the modest growth in the petals is expected after annealing the sample. As expected, there are no much morphological changes in the size of the pore and flowers of $CdMoS_4$. The average sizes of the hollow $CdMoS_4$ nanoflowers were observed to be in the range of 1.5-2 µm.

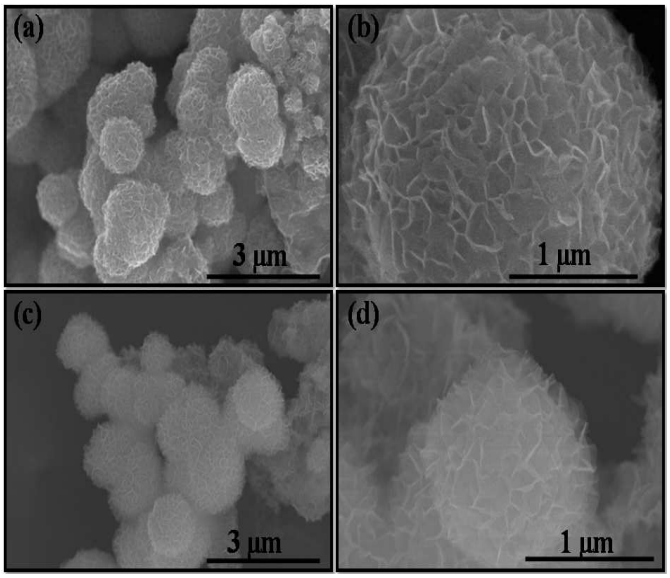

Figure 4. FESEM images of **(a-b)** as synthesized $CdMoS_4$ and**(c-d)** annealed $CdMoS_4$ at 400 °C.

The morphological and crystalline natures of the annealed $CdMoS_4$ samples were further characterized by TEM (Figure 5 a-d). The marigold nanoflower like structure is clearly seen in TEM images (Figure 5a-c). It is observed that nanoflower like structure obtained via self-assembling of thin curving petals. The morphology and size of the sample obtained from the TEM analysis matches well with the FESEM images depicted in Figure 4c-d. The Figure 5d shows the SAED pattern taken at the edge of the flakes shows the crystalline nature and monoclinic structure of the $CdMoS_4$ sample.

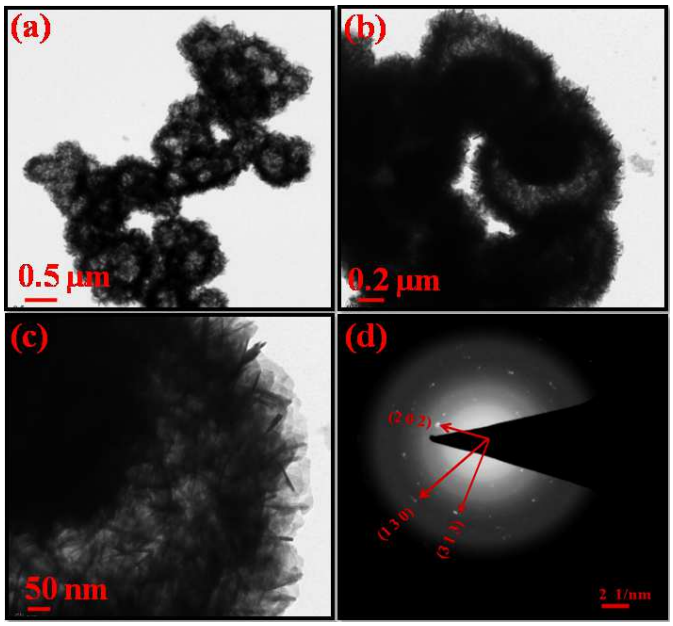

Figure 5. (a-c) TEM images and **(d)** SAED pattern of annealed $CdMoS_4$ at 400 °C nanoflower.

Further, the as synthesized and annealed samples were characterized using Raman spectroscopy. Raman spectroscopy is a very powerful and non-destructive technique widely used to

characterize various materials. It gives very precise and exact information about the change in bond distance and mechanical properties such as strain, stress, phase transition etc.[37-40] In view of this, as prepared and annealed samples were characterized by Raman spectroscopy and are shown in Figure 6a-c. In case of CdS, intense and broad peak at ~302, 603 and 903 cm^{-1} are assigned to fundamental optical phonon mode (LO) with the first overtone mode (2LO), and second overtone (3LO) of CdS, respectively (Figure 6c).[41] In case of annealed MoS_2, the Raman peaks at 382.5 and 406 cm^{-1} are identified as an E^1_{2g} and A_{1g} vibration mode matches well with earlier reports (Figure 6a).[42-43] These peaks belong to in-plane and out of plane vibration mode of typical MoS_2 sample. The width separation between two peaks is observed to be 23.5 cm^{-1} indicates the existence of few layer nature of MoS_2 which are also seen in FESEM (Figure 2). The other than E^1_{2g} and A_{1g} vibration mode of annealed MoS_2, new bands appeared in the as prepared MoS_2 phase which clearly shows the formation of 1T MoS2 phase.[44] As synthesized 1T MoS_2 (octahedral geometry) is a metastable phase (not stable) and transformed to 2H structure (trigonal prismatic geometry) after annealing at 400 ^oC (Figure 6b).[45] The intense Raman peak at 298, 430, 598 and 960 cm^{-1} are assigned for as prepared $CdMoS_4$ sample which is shown in supporting information ESI S-2(Figure S-1). Whereas, the peak at 125, 150, 182, 238, 285, 307, 398, 664, 754, 819, 860 and 890 cm^{-1} are assigned to annealed $CdMoS_4$ sample (Figure 6b). The Raman spectra of annealed $CdMoS_4$ sample do not show any signature of CdS or MoS_2 sample indicating the formation of single phase $CdMoS_4$.

The XPS analysis of annealed $CdMoS_4$ sample was also carried out and which is observed to be good agreement with stoichiometric phase formation. The XPS were used to investigate the chemical state of Cd, Mo and S in the 400^oC annealed $CdMoS_4$ sample. The Cd 3d, Mo 3d and S2p spectra of these samples are shown in Figure 7a-c. The Cd spectra showed two peaks with binding energy values of 404.9 and 411.7eV, which corresponds to Cd $3d_{5/2}$ and Cd $3d_{3/2}$ core level peaks respectively as reported earlier.[46] Similarly, Mo also shows two peaks having binding energy values of 228.8 and 232.1eV assign to Mo $3d_{5/2}$ and Mo $3d_{3/2}$ core level peaks respectively, which were characteristic feature of the tetragonal Mo^{+4}/Mo^{+6}.[47-49] Deconvolution of the XPS spectra by peak fitting revealed that the one Mo 3d doublets (228.4 and 229.1 eV) indicative of a mixed-valent (Mo^{4+} and Mo^{6+}) as shown in supporting information ESI: S-3 (Figure S-1a), which is in good agreement with earlier report.[50] Further, the area under curve reveal that percentage of Mo^{4+} and Mo^{6+} are found to be 37% and 63% respectively (for more details see supporting information ESI: S-3, Table S-1). The sulphur 2p spectra showed a peak at binding energy 161.6 eV, confirming the presence of sulfur.[46] Further, S2p peak deconvoluted into three peaks at binding energies 161.0, 161.6 and 162.4 eV assigned to CdS, MoS_2 and MoS_3 species (see supporting information ESI: S-3, Figure S-1b).[47,51-52] Our XPS measurements established the formation of stable $CdMoS_4$ phase along with occasional $CdMoS_{4-x}$ phase.

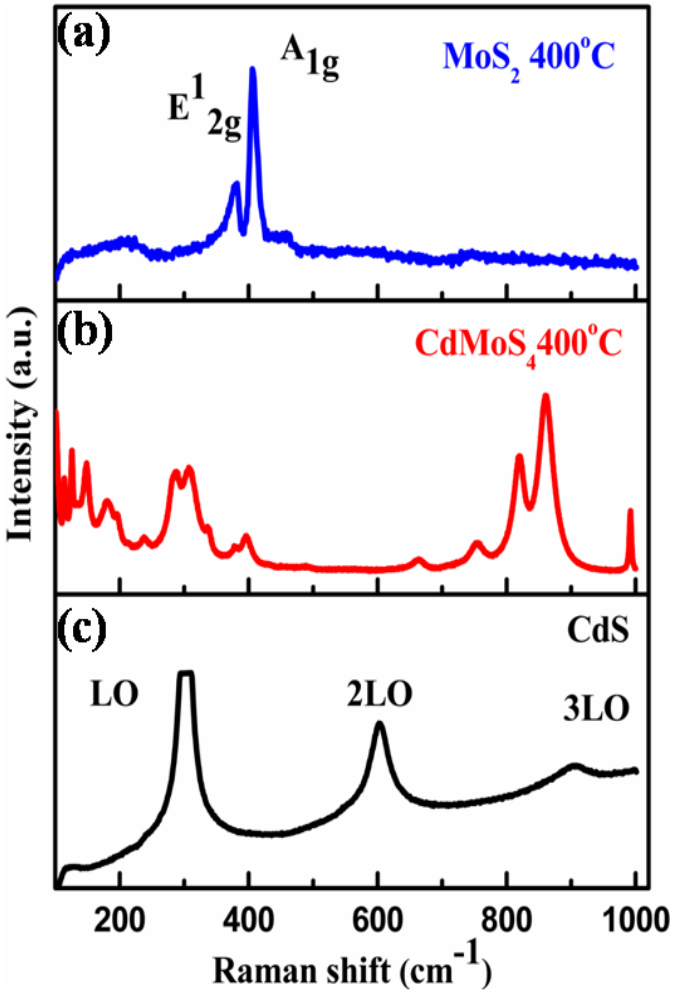

Figure 6. (a) Raman spectrum of as prepared CdS, **(b)** annealed $CdMoS_4$ and **(c)** annealed MoS_2.

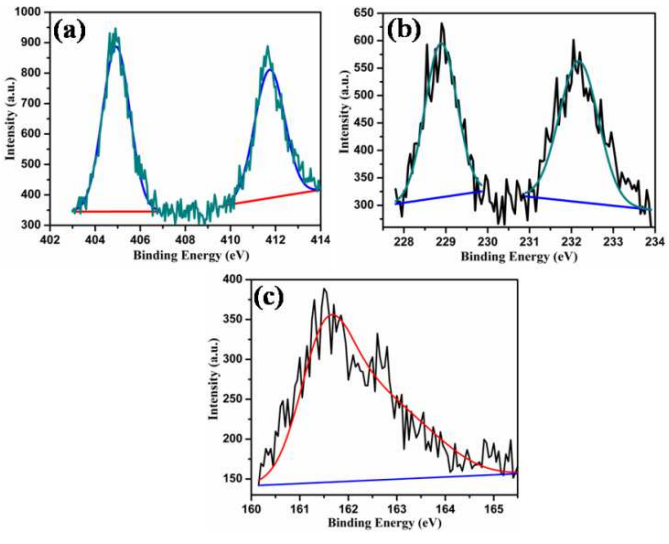

Figure 7. (a) Cd 3d, (b) Mo 3d and (c) S 2P XPS spectra of $CdMoS_4$ annealed at 400 ^oC samples.

The as synthesized CdS, MoS_2, $CdMoS_4$, and annealed MoS_2, $CdMoS_4$, samples were further characterized by UV-Vis spectroscopy as shown in Figure 8a-b. It is observed that the as

prepared CdS, MoS_2 and $CdMoS_4$ samples show the absorption edge cut off at ~510 (2.44 eV), 487 (2.55 eV) and 497 nm (2.50 eV), respectively. In case of annealed MoS_2 and $CdMoS_4$ (400 ^oC for 4 hrs), red shift in absorption edge has been observed. The annealed samples of MoS_2 and $CdMoS_4$ shows band gap of 1.6 and 1.5 eV respectively. In case of MoS_2, this may be due to decrease in the size and stacking of sheets and/or due to the structure transformation into 2H MoS_2.[53] It is quite obvious that $CdMoS_4$ may have such geometry as per the absorption behaviour.

The PL investigations are useful for analysis of migration, transfer, and recombination processes of photo induced electron–hole pairs in a semiconductor material. The room temperature PL spectra of the as synthesized and annealed samples were recorded with an excitation wavelength of 350 nm and are shown in Figure 8c,d. The CdS sample shows the broad emission peak at 630 nm and other low intensity shoulder peak shows at 644 nm. The strong orange emission obtained at 630 nm and other low intensity emission is attributed to the surface state defects or clustering of nanoparticles.[54-56] In case of MoS_2 emission peak at 627 nm is due to the band edge transition which matches with earlier reports in literature.[57] The $CdMoS_4$ sample shows almost same intensity peak at 628 nm. The weak peak at 645 nm in $CdMoS_4$ sample is also due to the surface state defects.

The self-assemblies of 2D and 3D nanostructures have the predominant degree of clustering which also gives such weak broad peak. The intensity of PL emission peaks for MoS_2 and $CdMoS_4$ sample are much lower than that of CdS sample which indicates presence of more defects. This indicates that there is a great inhibition of electron (e^-) and hole (h^+) recombination in case of MoS_2 and $CdMoS_4$ sample.

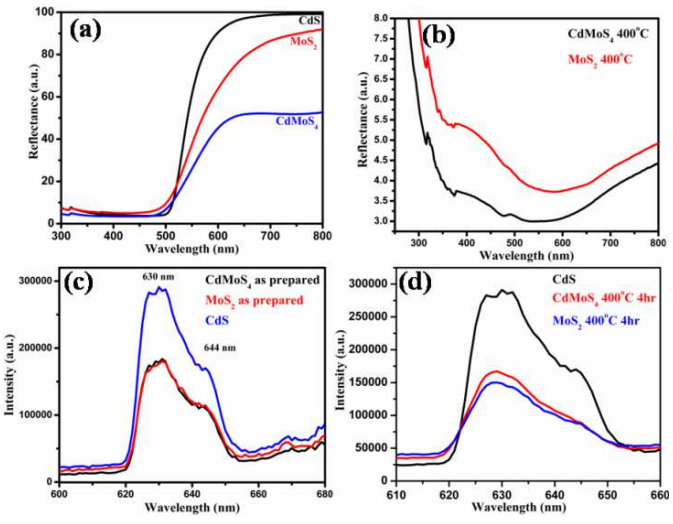

Figure 8. (a) Reflectance spectra of as synthesized CdS, $CdMoS_4$ and MoS_2. (b) Reflectance of $CdMoS_4$ and MoS_2 after annealing. (c) Photoluminescence spectra of as synthesized CdS, $CdMoS_4$ and MoS_2. (d) Photoluminescence spectra of as synthesized CdS, annealed $CdMoS_4$ and MoS_2 at 400 ^oC for 4 hours.

3.1 Formation mechanism of MoS_2 Nanosheet and $CdMoS_4$ nanoflower:

The MoS_2 nanosheets were prepared solvothermally using ammonium molybdate and thiourea in the methanol medium. During the solvothermal process, the ammonium ions and molybdenum ions are formed. Further these molybdate ions are reacting with thiourea and form MoS_4^{2-} ions as per the following reaction.[58]

$$MoO_4^{2-} + NH_2CSNH_2 \longrightarrow MoS_4^{2-} \quad (1)$$

During the reaction the ammonium ions slowly decompose into NH_3 and H^+ ions. These H^+ ions are reacting with $MoS_4^{2-}$and gives 1T phase of MoS_2 as per the following reaction.[56]

$$MoS_4^{2-} + 4H^+ \longrightarrow MoS_2 + 2H_2S \quad (2)$$

The as prepared MoS_2 nanosheet sample were1T phase and it is observed that after annealing the sample at 400 ^oC, it transform to stable MoS_2 (2H phase) which has been discussed earlier in this manuscript.

The $CdMoS_4$ samples were prepared using identical condition with cadmium nitrate as source material. The $CdMoS_4$ nanoflowers were formed proceeding through reaction (1) as per the following reaction.

$$Cd^{2+} + MoS_4^{2-} \longrightarrow CdMoS_4 \quad (3)$$

The above as prepared $CdMoS_4$ nanoflower sample were annealed at 400 ^oC to confirm the formation of stable $CdMoS_4$ phase. Surprisingly, we did not observe any change in the surface morphology of as prepared and annealed MoS_2 and $CdMoS_4$ samples at 400 ^oC except puffiness of the nanoflowers in case of $CdMoS_4$.

The schematic representation of growth mechanism for MoS_2 is shown in scheme 1. At hydrothermal condition, the MoS_4^{2-} ions are slowly reduced to form MoS_2. Primarily, the MoS_2 nuclei's in supersaturated solution are formed at hydrothermal conditions. These nuclei further grow and form the thin layered hexagonal nanoparticles by typical crystal growth mechanism *i.e.* Ostwald ripening process (Scheme 1a). Due to prolong hydrothermal reaction time, there is a 2D anisotropic growth of these thin hexagonal nanoparticles by oriental attachment and form a bigger thin layer MoS_2 sheets (Scheme 1b). Initially, the growth is quite faster due to the high concentration of MoS_2 nuclei and hence long sheets were formed. As hydrothermal reaction proceeds with time, the concentration of MoS_2 nuclei's in the reaction slows down, which confer the formation of smaller MoS_2 hexagonal cell with 2D vertical growth on bigger sheets (which also acts as a seed). Significantly, in the later stage of the hydrothermal reaction, the smaller vertically grown hexagonal thin nanosheets self-organized and form honeycomb like structure (Scheme 1c) with hexagonal cavity. This is a very unique structure obtained in this manuscript, not reported so far in the literature for the MoS_2. It is well known that such 2D growth and self-assembly is strongly related to the intrinsic structure of pristine MoS_2. Hence, honeycomb like structure with hexagonal cavity is quite justifiable. We observed that the stability of 1T

MoS_2 and as prepared $CdMoS_4$ is very poor as they immediately dissolved in slightly alkaline medium. However, annealed 2H MoS_2 sample are very stable in alkaline condition.

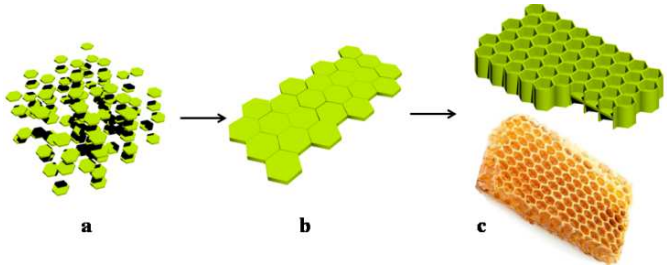

Scheme 1. Formation of Honeycomb structure of MoS_2. (a) Hexagonal nanosheets (b) monolayer of MoS_2 (c) MoS_2 Honeycombs.

The growth mechanism proposed for $CdMoS_4$ is somewhat similar but instead of honeycomb we obtained marigold nanoflower like structure. Initially, tiny nuclei of $CdMoS_4$ are generated as per the reaction (3) in the supersaturated solution and further growth of nanoparticles takes place with time (Scheme 2a). These newly formed nanoparticles are spontaneously aggregated to minimize their surface energy. These nanoparticles further grow anisotropically along the 3D directions and resulting in the formation of plane nanosphere of size 1.5 µm (Scheme 2b). At prolonged hydrothermal reaction, further growth is hindered due to the reduction in the precursor concentration. Hence, with prolong reaction time (36 hr), there is formation of slightly open nanoflower (scheme 2c). Whereas at 48 hr reaction time, there is formation of a 3D hierarchical nanostructure *i.e.* marigold nanoflowers.(Scheme 2d). Further, we studied the photocatalytic hydrogen evolution from H_2S using annealed MoS_2 and $CdMoS_4$ nanostructures.

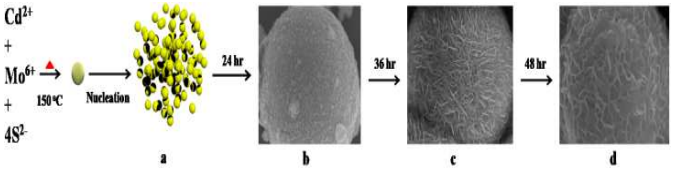

Scheme 2. Formation of marigold flower of $CdMoS_4$. (a) $CdMoS_4$ NPT (b) self-assembled $CdMoS_4$ nanosphere (c) Slightly open $CdMoS_4$ nanosphere (4) $CdMoS_4$ Marigold nanoflower.

3.2 Photocatalytic study:

We performed photocatalytic activity for H_2 production from copious H_2S. Photocatalytic H_2 production experiments were conducted using as prepared CdS, MoS_2 and $CdMoS_4$ under visible light irradiation. Table1 summarizes the results of photocatalytic activity for H_2 generation by photodecomposition of H_2S using as prepared CdS, annealed MoS_2 and $CdMoS_4$ nanostructure samples. The as prepared MoS_2 and $CdMoS_4$ sample did not show any photocatalytic activity due to the instability in alkaline medium. As discussed earlier, the structure of the as synthesized MoS_2 and $CdMoS_4$ itself is not stable and hence it gets degraded during the photocatalytic reaction. The annealed MoS_2 and $CdMoS_4$ show superior and stable cyclic performance with ±0,1 % accuracy of activity due to the structural stability of these catalysts. It is important to note that all the experiments reported in this manuscript were carried out at an identical condition. The comparative time dependent photocatalytic H_2 production activities are shown in Fig. 9. The utmost H_2 production *i.e.* 10300, 12555 and 25445 µMole $h^{-1}g^{-1}$ were obtained for as prepared CdS, annealed MoS_2 and $CdMoS_4$, respectively. It is noteworthy that MoS_2 and $CdMoS_4$ sample have rendered significant photocatalytic activity, which is much higher than that of CdS samples reported in present work and previously reported nanostructures of CdS/CdS-MoS_2.[25,32,59-61]

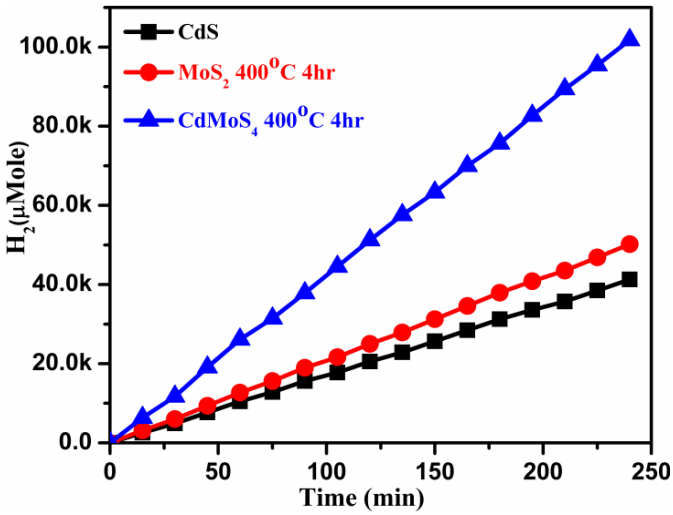

Figure 9. Photocatalytic H_2 generation activity plot by H_2S splitting for CdS, MoS_2 400 °C and $CdMoS_4$ 400 °C.

Table 1: Hydrogen generation from H_2S splitting.

Sr. No.	Catalyst used	Average H_2 generated (µMole)	% Apparent quantum yield
1	CdS	10320	14.54
2	MoS_2 400 °C 4 hr	12555	17.68
3	$CdMoS_4$ 400 °C 4 hr	25445	35.84

Considering the band gap of annealed MoS_2, $CdMoS_4$ and the as synthesized CdS, the higher activity obtained for $CdMoS_4$ is quite understood. Recently, Hinnemann *et al.* has demonstrated that MoS_2 nanostructure material is good photocatalyst for H_2 production.[62] Additionally, the edge sites of MoS_2 and vacancy defects were found to be responsible for the photocatalytic activity.[63-64] It is well known that the morphology of the material plays an crucial and important role in the context of photocatalysis.[34,65-66] The FESEM and TEM image of the MoS_2 clearly shows the honeycomb like mesoporous structure. Further, the PL investigations, were also carried out which showed the vacancy defects in both the materials which ultimately suppress the recombination of photo

generated charge carrier, significantly. Hence, the enhanced photocatalytic H_2 production activity were obtained for the naked nanostructured MoS_2 (Honeycomb) is quite justifiable. Singh *et al.* has proved that MoS_2 nanosheet gives good H_2 evolution as compared to the bulk sample.[53] In the present case, we utilized few layers of MoS_2 nanosheets with honeycomb structure which has good stability along with short carrier diffusion time and hence shows good performance to photocatalytic activity for hydrogen production.[67] Additionally, for MoS_2 honeycomb structure (vertically grown hexagons) may be helping the fast transport of photo generated carriers to the surface which also responsible for enhanced H_2 production as compared to CdS. Interestingly, the $CdMoS_4$ nanoflower sample show almost double H_2 production performance as compared to CdS and MoS_2 sample. The previous reports of CdS and CdSe-MoS_2 hetero structure with 0.2 % MoS_2 shows good photocatalytic activity due to the inter electron transfer (CdS/MoS_2 composites).[68] However, it decreases with increasing MoS_2 concentration and reason for that is still unknown.[68] Interestingly, in the present case, single phase $CdMoS_4$ confer higher H_2 production activity with 35.84 % quantum efficiency. We propose that the morphology of the $CdMoS_4$ as compared with MoS_2 play the important role for enhanced H_2 production. Further, the morphology of $CdMoS_4$ is a porous marigold nanoflower like structure and we have demonstrated that the nanoflower like morphology confer good photocatalytic activity.[32] The self-assembly of nanoflowers is from the thin petals which has more open surface area for absorption of light and hence produce more number of charge carriers. The electron transfer to the surface is quite easy due to the thin nanosheets or nanopetals like morphology of the sample which inhibit charge recombination. Interestingly, these nanoflowers are hollow and are observed to be highly crystalline in nature, which may also accountable for the enhanced photocatalytic activity.[7] As discussed, flower like morphology (3D structure) has more advantage of fast electron transport to the surface as compared to Honeycomb structure. The vertically grown petals in honeycomb structure (2D structure) are accelerating electron transport to the surface but not fast as compared to 3D flower like structure. These structures have significance in the electron transport and mobility.[32.]

This is the only report which demonstrates the enhanced H_2 production by photocatalytic H_2S decomposition using $CdMoS_4$ nanoflower and honeycomb like MoS_2 nanostructure as a catalyst under visible light irradiation. The stability of the catalyst confirmed by performing recycles studies and which shows reproducibility of the results. The XRD of the reused sample catalyst did not depict any change in the phase purity of $CdMoS_4$ and MoS_2, which also indicates that the catalysts used for H_2 production are highly stable (see supporting information ESI S-4 Figure S1-S2). We did not found any H_2 production in the absence of catalyst and in the dark condition (without light). Overall, it is observed that the $CdMoS_4$ and MoS_2 samples are quite stable under the visible light and are acts as an active photocatalysts. The mechanism of hydrogen generation is explained as below:

$$H_2S + HO^- \longleftrightarrow HS^- + H_2O$$

$$\text{Semiconductor} \xrightarrow{h\nu} h^+ VB + e^- CB$$

$$\text{Oxidation reaction: } 2HS^- + 2h^+VB \longrightarrow S_2^{2-} + 2H^+$$

$$\text{Reduction reaction: } 2H^+ + 2e^- CB \longrightarrow H_2$$

The H_2S splitting under visible light takes place as follows. In 0.25 M KOH solution with pH 12.5 (pKa= 7.0) and the weak diprotic acid H_2S (pKa= 11.96) dissociates maintaining an equilibrium with HS^- ions. The $CdMoS_4$ and MoS_2 absorb the visible light and generate the e^- and h^+. Due to the mesoporous structure, generated e^- and h^+ easily goes to the surface of the catalyst and eagerly available for the photocatalytic activity. The photogenerated h^+ from catalyst in valence band oxidizes the SH^- ion to proton (H^+) and disulfide (S_2^{2-}) ion. The photogenerated e^- in conduction band from the catalyst generates the molecular H_2 by reducing the H^+. The reaction solution was always kept in the sulfide atmosphere by supplying the continuous bubbling of H_2S. The blank run without H_2S did not give any H_2 production indicates that H_2 production is from H_2S but not from water at similar experimental conditions.

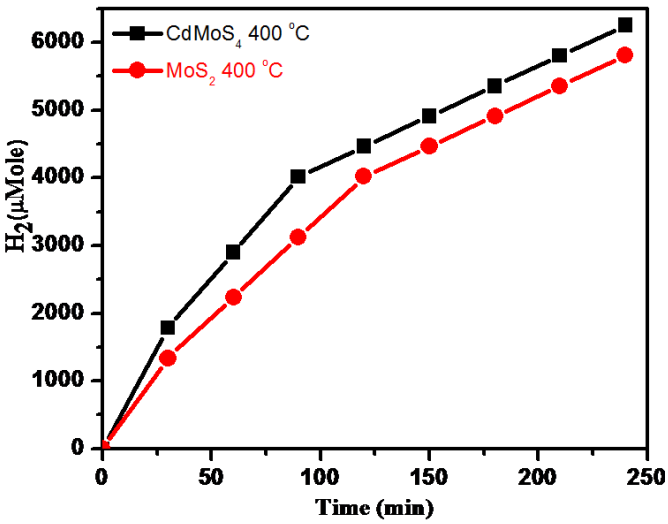

Figure 10 Photocatalytic H_2 generation from water with existence of sacrificial reagents using $CdMoS_4$ 400 °C and MoS_2 400 °C.

Table 2: Hydrogen generation from H_2O splitting

Sr. No.	Catalyst used	Average H_2 generated With Methanol (µMole)	Average H_2 generated Without Methanol (µMole)
1	$CdMoS_4$ 400 °C 4 hr	1562.5	919.1
2	MoS_2 400 °C 4 hr	1450.8	806

We have also attempted the water splitting experiment using 2D MoS_2 sheets and 3D $CdMoS_4$ nanoflower as an active

catalyst in the presence of UV-visible light. The highest H_2 production achieved by photocatalytic water splitting was 1562.5 and 1450.8 µMole $h^{-1}g^{-1}$ for $CdMoS_4$ and MoS_2, respectively. The time dependent H_2 production results were shown in Figure 10 and the H_2 production rate were given in Table 2. In the present investigations, we have used methanol as a sacrificial reagent. The methanol suppresses the evolution of oxygen through formation of free radicals. The photo-generated electron reduced the H^+ ions to form H_2 gas while the hole react with water molecule to form ·OH radical. These ·OH radicals are reacting with CH_3OH and form $\cdot CH_2OH$ and H_2O. The use of methanol as a sacrificial reagents and its mechanism is also discussed earlier by F. Guzman *et al.*[69] The hydrogen evolution without methanol as a scarifying agent was observed to be very low (See ESI:S-5, Figure S-1 and Table 2) which clearly indicates the significance of methanol. The low H_2 production rate for water splitting as compared to the H_2S is quite obvious due to the thermodynamics of water splitting. In nutshell, typically the morphology is responsible for the enhanced H_2 production. The MoS_2 has given comparable H_2 production because of the good photocatalytic ability for oxidation as well as reduction as reported earlier for few layered MoS_2.[53] We have demonstrated the detail investigation of the H_2 production from H_2S and attempted to compare with water splitting results. Overall, it is noteworthy that the MoS_2 honeycomb structure and newly design $CdMoS_4$ 3D marigold nanoflower demonstrates good H_2 production.

4. Conclusion

In conclusion, we have demonstrated the 2D honeycomb MoS_2 nanosheet and 3D nanostructure marigold flowers of $CdMoS_4$ with formation and growth mechanism. The annealing of samples at 400 ^oC confers very stable structures of (2H) MoS_2 and $CdMoS_4$ nanoflower. The photocatalytic H_2 production from H_2S and water splitting investigated for the annealed MoS_2 and $CdMoS_4$ samples. The $CdMoS_4$ exhibited enhanced H_2 production as compared to MoS_2, as the morphology of the catalysts plays an important key role in the enhancement of H_2 production. The generated e^- transfer to the surface is quite easy due to the thin nanosheets and nanopetals like morphology which inhibit charge recombination. Additionally, the surface defects generated by these nanostructures inhibit the charge carrier recombination. Our results open up several new avenues for utilization of MoS_2, $CdMoS_4$ and several other 2D layered TMDCs nanostructure materials for enhanced photocatalytic activity. The MoS_2 honeycomb like structure and newly design 3D $CdMoS_4$ marigold nanoflower will have potential to be used in other optoelectronic and energy harvesting devices.

Acknowledgements

Authors would like to thank Prof. C. N. R. Rao (FRS) (Director ICMS, Bangalore, India) and Prof. Vinayak P. Dravid (Director, NUANCE NWU, USA) for support and encouragement. Dr. D. J. Late would like to thank Department of Science and Technology (Government of India) for Ramanujan Fellowship Grant No. SR/S2/RJN-130/2012 and DST-SERB Fast-track Young scientist project Grant No. SB/FT/CS-116/2013 and MLP 028626. Mr. Sunil Kadam would like to thank Department of Science and Technology and Department of Electronics and Information Technology (DeitY), Government of India, for the financial support. Dr. Bharat B. Kale and Prof. Chan-Jin Park would like to acknowledge the support by MSIP (Ministry of Science, ICT & future planning), Korea through Brain Pool program. Dr. Bharat B. Kale also thankful to Centre for Materials for Electronics Technology (C-MET), Pune for implementation of the project. Thanks for Dr. S. Arbuj for help in water splitting activity experiment.

Notes and references

[a]*Centre for Materials for Electronics Technology (C-MET), Department of Electronics and Information and Technology (DeitY), Government of India, Panchawati off Pashan road, Pune –411008, India :* ***kbbb1@yahoo.com***
[b]*Physical and Materials Chemistry Division, CSIR-National Chemical Laboratory, Dr. HomiBhabha Road, Pune 411008, Maharashtra, India*
[c]*Department of Physics, University of Pune -411007, India.*
[d]*Material Science & Engineering Department, Chonnam National University, Gwangju 500 757, South Korea*

1 L. Yin, Z. Zhang, Z. Li, F. Hao, Q. Li, C. Wang, R. Fan, Y. Qi, *Adv. Funct. Mater.* 2014, **24**, 4176.
2 S. Lee, V. Sridhar, J. Jung, K. Karthikeyan, Y. Lee, R. Mukherjee, N. Koratkar, K. Oh, *ACS Nano.* 2013, **7**, 4242.
3 D. J. Late, B. Liu, H. S. S. R. Matte, V. P. Dravid, C. N. R. Rao, *ACS Nano*, 2012, *6*, 5635.
4 D. J. Late,Y. Huang, B. Liu, J. Luo, J. Acharya, S. N. Shirodkar, J. Luo, A. Yan, D. Charles, U. V. Waghmare, V. P. Dravid, C. N. R. Rao, *ACS Nano*, 2013**, 7**, 4879.
5 R. Chalasani and S. Vasudevan, *ACS Nano*, 2013, **7**, 4093.
6 F. Withers, T. H. Bointon, M. F. Craciun and S. Russo, *ACS Nano*, 2013, **7**, 5052.
7 R. P. Panmand, Y. A. Sethi, S. R. Kadam, M. S. Tamboli, L. K. Nikam, J. D. Ambekar, C. J. Park and B. B. Kale, *CrystEngComm.*, **2**014, **17**, 107.
8 J. A. Turner, *Science*, 2004, *305*, 972.
9 W. Lubitz and B. Tumas, *Chem. Rev.*, 2007, **107**, 3900.
10 R. M. Navarro, M. A. Peña and J. L. G. Fierro, *Chem. Rev.*, 2007, **107**, 3952.
11 A. Kudo, *Pure Appl. Chem.*, 2007, **79**, 1917.
12 I. A. Gargurevich, *Ind. Eng. Chem. Res.*, 2005, **44**, 7706.
13 G. Liu, X. Jiao, Z. Qina and D. Chen, *CrystEngComm,*, 2011, **13**, 182.
14 X. Chen, C. Li, M. Grätzel, R. Kostecki and S. S. Mao, *Chem. Soc. Rev.*, 2012, **41**, 7909.
15 M. P. Elsner, M. Menge, C. Muller and D. W. Agar, *Catal. Today*, 2003, **79**, 487.
16 H. Lu, J. Zhao, L. Li, L. Gong, J. Zhang, L. Zhang, Z. Wang, J. Zhang and Z. Zhu, *Energy Environ. Sci.*, 2011, **4**, 3384.
17 N. Jiawei, S. Xu, X. Zhang, H. Y. Yang and D. D. Sun, *Adv. Funct. Mater.*, 2010, **20**, 4287.
18 S. R. Kadam, V. R. Mate, R. P. Panmand, L. K. Nikam, M. V. Kulkarni, R. Sonawane and B. B. Kale, *RSC Adv.*, 2014, **4**, 60626.
19 L. Zhang, W. Wang, S. Sun, D. Jianga and E. Gaoa, *CrystEngComm.*, 2013, **15**, 10043.
20 S. Iyyapushpam, S.T. Nishanthi and D. P. Padiyan, *Materials Letters*, 2012, **86**, 25.

21 S. Ho-Kimura, S. J. A. Moniz, A. D. Handokoa and J. Tang, *J. Mater. Chem. A*, 2014, **2**, 3948.
22 L. Chen, E. Alarcón-Lladó, M. Hettick, I. D. Sharp, Y. Lin, A. Javey and J. W. Ager, *J. Phys. Chem. C*, 2013, **117(42)**, 21635.
23 (a)Y. Chen, C. Lu, L. Xu, Y. Ma, W. Hou and J. J. Zhu, *CrystEngComm*, 2010, **12**, 3740. (b) K. B. Gawande, S. B. Gawande, S. R. Thakare, V. R. Mate, S. R. Kadam, B. B. Kale, M. V. Kulkarni, *RSC Advances*, 2015, **5**, 40429.
24 N. S. Chaudhari, S. S. Warule, S. A. Dhanmane, M. V. Kulkarni, M. Valant and B. B. Kale, *Nanoscale*, 2013, **5**, 9383.
25 S. K. Apte, S. N. Garaje, G. P. Mane, A. Venu, S. D. Naik, D. P. Amalnerkar and B. B. Kale, *Small*, 2011, **7**, 957.
26 S. R. Lingampalli, U. K. Gautam and C. N. R. Rao, *Energy Environ. Sci.*, 2013, **6**, 3589.
27 Y. Li, G. Chen, Q. Wang, X. Wang, A. Zhou and Z. Shen, *Adv. Funct. Mater.*, 2010, **20,** 3390.
28 J. Zhang, J. Yu, Y. Zhang, Q. Li and J. R. Gong, *Nano Lett.*, 2011, **11**, 4774.
29 (a) U. V. Kawade, R. P. Panmand, Y. A. Sethi, M. V. Kulkarni, S. K. Apte, S. D. Naik and B. B. Kale, *RSC Adv.*, 2014, **4**, 49295. (b) S. R Kadam, R. P Panmand, R. S Sonawane, S. W Gosavi, B. B. Kale, *RSC Advances*, 2015, **5**, 58485.
30 Q. Li, B. Guo, J. Yu, J. Ran, B. Zhang, H. Yan and J. R. Gong, *J. Am. Chem. Soc.*, 2011, **133**, 10878.
31 G. Ma, H. Yan, J. Shi, X. Zong, Z. Lei and C. Li, *J. Catal.*, 2008, **260**, 134.
32 (a) B. B. Kale, J. O. Baeg, S. M. Lee, S. J. Changand and C. W. Lee, *Adv. Funct. Mater*, 2006, **16**, 1349. (b) N. S. Chaudhari, S. S. Warule, S. A. Dhanmane, M. V. Kulkarni, M. Valant and B. B. Kale, *Nanoscale*, 2013, **5**, 9383.
33 N. S. Chaudhary, A. P. Bhirud, R. S. sonawane, L. K. Nikam, S. S. Warule, V. H. Rane and B. B. Kale, *Green Chem.,* 2011, **13**, 2500.
34 S. K. Apte, S. N. Garaje, R. D. Bolade, J. D. Ambekar, M. V. Kulkarni, S. D. Naik, S. W. Gosavi, J. O. Baegand B. B. Kale *J.Mater.Chem.*, 2010, **20**, 6095.
35 F. Dapeng, L. Weimin and X. Quaji, *Chinese J. Material Research,* 2001, **15(3)**, 367.
36 N. Dragoe, *J. Appl. Cryst.*, 2001, **34**, 535.
37 (a) D. J. Late, U. Maitra, L. S. Panchakarla, U. V. Waghmare and C. N. R. Rao, *J. Phys.: Condens. Matter*, 2011, **23**, 055303. (b) I. Calizo, A. A. Balandin, W. Bao, F. Miao and C. N. Lau, *Nano Lett*, 2007, **7**, 2645.
38 (a) D. J. Late, B. Liu, H. S. S. Matte, C. N. R. Rao, V. P. Dravid, *Adv. Funct. Mater.* 2012, **22**, 1894. (b) M. Thripuranthaka, D. J. Late, *ACS Appl. Mater. Interfaces.* 2014, **6**, 1158. (c) D. J. Late, S. N. Shirodkar, U. V. Waghmare, V. P. Dravid, C. N. R. Rao, *ChemPhysChem*, 2014, **15**, 1592. (d) D. J. Late, T. Doneux, M. Bougouma, *App. Phys. Lett.* 2014, **105**, 233103
39 S. Chen, Q. Wu, C. Mishra, J. Kang, H. Zhang, K. Cho, W. Cai, A. A. Balandin and R. S. Ruoff, *Nature Mater.*, 2012, *11*, 203.
40 A. A. Balandin, *Nature Mater.* 2011, **10**, 569.
41 A. Abdi, L. V. Titova, L. M. Smith, H. E. Jackson, J. M. Yarrison-Rice, J. L. Lensch and L. J. Lauhon, *Appl. Phys. Lett.*, 2006, **88**, 043118.
42 H. Li, Q. Zhang, C. C. R. Yap, B. K. Tay, T. H.T. Edwin, A. Olivier and D. Baillargeat, *Adv. Funct. Mater.*, 2012, **22**, 1385.
43 M. Thripuranthaka, R. V. Kashid, C. S. Rout and D. J. Late, *Appl. Phys. Lett.*, 2014, **104**, 081911.
44 C. N. R. Rao, U. Maitra and U. V. Waghmare, *Chem. Phys. Lett.*, 2014, **609**, 172.
45 G. Eda, T. Fujita, H. Yamaguchi, D. Voiry, M. Chen and M. Chhowalla, *ACS Nano*, 2012, **6**, 7311.
46 M. Marychurch and G.C.Morris, *Surf. Sci.*, 1985, **154**, L251.
47 L. Benoist, D. Gonbeau, G. Pfister-Guillouzo, E. Schmidt, G. Meunier and A. Levasseur, *Surf. Interface Anal.*, 1994, **22**, 206.
48 A. Cimino and B. A. De Angelis, *J. Catal.*, 1975, **36**, 11.
49 J. S. Muijsers, T. Weber, R. M. vanhardeveld, H. W. Zandbergen and J. W. Niemantsverdriet, *J. Catal.*, 1995, **157**, 698.
50 T. M. McEvoy and Stevenson, *J. Mater. Res.*, 2004, **19**, 429.
51 E. Agostinelli, C. Battistoni, D. Fiorani, G. Mattogno and M. Nogues, *J. Phys. Chem. Solids*, 1989, **50**, 269.
52 T. I. Koranyi, I. Manninger, Z. Paal, O. Marks and J. R. Gunter, *J. Catal.*, 1989, **116**, 422.
53 N. Singh, G. Jabbour and U. Schwingenschlogl, *Eur. Phys. J. B.*, 2012, **85**, 392.
54 K. Fujihara, S. Izumi, T. Ohno and M. Matsumura, *Photochem. Photobiol. A: Chem.*, 2000, **132**, 99.
55 J. Tang, Z. Zou and J. Ye, *J. Phys. Chem.B.*, 2003, **107**, 14265.
56 M. Pal, N. R. Mathews, P. Santiago and X. Mathew, *J. Nanopart. Res.*, 2012, **14**, 916.
57 X. Huang, Z. Zeng and H. Zhang, *Chem. Soc. Rev.*, 2013, **42**, 1934.
58 W. Chen, H. Chen, H. Zhu, Q. Gao, J. Luo, Y. Wang, S. Zhang, K. Zhang, C. Wang, Y. Xiong, Y. Wu, X. Zheng, W. Chu, L. Song and Z. Wu, *Small*, 2014, **10**, 4637.
59 Q. Wang, J. Li, Y. Bai, J. Lian, H. Huang, Z. Li, Z. Lei, W. Shangguan, *Green Chem.* 2014, **16**, 2728.
60 S. K. Apte, B. B. Kale, R. S. Sonawane, S. D. Naik, S. S. Bodhale and B. K. Das, *Mater. Lett.*, 2006, **60**, 499.
61 T. S. Jia, A. Kolpin, C. Ma, R. C. T. Chan, W. M. Kwokc and S. C. E. Tsang, *Chem. Commun.*, 2014, **50**, 1185.
62 B. Hinnemann, P. G. Moses, J. Bonde, K. P. Jørgensen, J. H. Nielsen, S. Horch, I. Chorkendorff and J. K. Nørskov, *J. Am. Chem. Soc.*, 2005, **127**, 5308.
63 T. F. Jaramillo, K. P. Jørgensen, J. Bonde, J. H. Nielsen, S. Horch and I. Chorkendorff, *Science*, 2007, **317**, 100-102.
64 C. Ataca, and S. Ciraci, *Phys. Rev. B,* 2012, **85**, 195410.
65 X. F. Cao, L. Zhang, X. T. Chen and Z. L. Xue, *CrystEngComm*, 2011, **13**, 306-311.
66 R. Chen, J. Bi, L. Wu, Z. Li and X. Fu, *Cryst. Growth Des.*, 2009, **9**, 1775-1779.
67 B. L. Abbrams and J. P. Wilcoxon, *Crit. Riv. Solid State Mater. Sci.*, 2005, **30**, 153.
68 J. Zhang, Z. Zhu, X. Feng, *Chem. Eur. J.* 2014, **20**, 1–5.
69 F. Guzman, S. S. C. Chuang, and C. Yang, *Ind. Eng. Chem. Res.* 2013, **52**, 61.

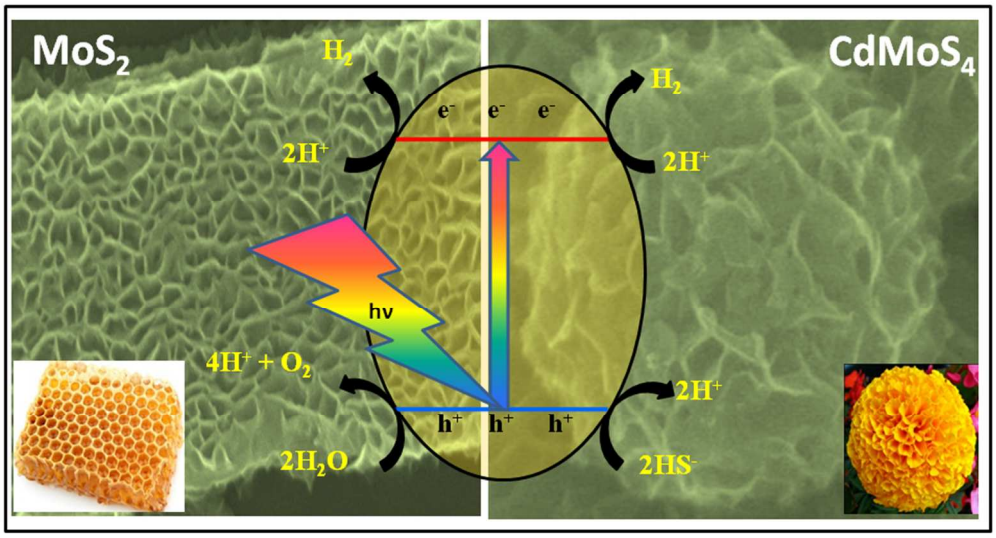

254x190mm (96 x 96 DPI)